ADVANCES IN ATMOSPHERIC SCIENCES, VOL. 34, JANUARY 2017, 66–78

• **Original Paper** •

Impact of Coastal Radar Observability on the Forecast of the Track and Rainfall of Typhoon Morakot (2009) Using WRF-based Ensemble Kalman Filter Data Assimilation

Jian YUE[1], Zhiyong MENG*[1], Cheng-Ku YU[2], and Lin-Wen CHENG[2]

[1]*Laboratory for Climate and Ocean–Atmosphere Studies, Department of Atmospheric and Oceanic Sciences, School of Physics, Peking University, Beijing* 100871

[2]*Department of Atmospheric Sciences, NTU, Taipei* 10617

(Received 28 January 2016; revised 17 August 2016; accepted 9 September 2016)

ABSTRACT

This study explored the impact of coastal radar observability on the forecast of the track and rainfall of Typhoon Morakot (2009) using a WRF-based ensemble Kalman filter (EnKF) data assimilation (DA) system. The results showed that the performance of radar EnKF DA was quite sensitive to the number of radars being assimilated and the DA timing relative to the landfall of the tropical cyclone (TC). It was found that assimilating radial velocity (Vr) data from all the four operational radars during the 6 h immediately before TC landfall was quite important for the track and rainfall forecasts after the TC made landfall. The TC track forecast error could be decreased by about 43% and the 24-h rainfall forecast skill could be almost tripled. Assimilating Vr data from a single radar outperformed the experiment without DA, though with less improvement compared to the multiple-radar DA experiment. Different forecast performances were obtained by assimilating different radars, which was closely related to the first-time wind analysis increment, the location of moisture transport, the quasi-stationary rainband, and the local convergence line. However, only assimilating Vr data when the TC was farther away from making landfall might worsen TC track and rainfall forecasts. Besides, this work also demonstrated that Vr data from multiple radars, instead of a single radar, should be used for verification to obtain a more reliable assessment of the EnKF performance.

Key words: radial velocity, ensemble Kalman filter, observability, tropical cyclone, track, rainfall

Citation: Yue, J., Z. Y. Meng, C.-K. Yu, and L.-W. Cheng, 2017: Impact of coastal radar observability on the forecast of the track and rainfall of Typhoon Morakot (2009) using WRF-based ensemble Kalman filter data assimilation. *Adv. Atmos. Sci.*, **34**(1), 66–78, doi: 10.1007/s00376-016-6028-8.

1. Introduction

Considering the maximum range of radial velocity (Vr) measurements of a coastal radar is only 230 km, although assimilating coastal radar Vr data when a tropical cyclone (TC) enters the radar data coverage region does not have much lead time for the landfalling forecast, it may be important in improving TC track and rainfall forecasts after the TC makes landfall. Heavy rainfall that happens inland after TC landfall often causes huge disasters, such as Typhoon Bilis (2006) and Typhoon Morakot (2009). At present, the operational rainfall forecast skill associated with landfalling TCs is very low (e.g., Gao et al., 2009; Huang et al., 2011). Thus, coastal radar data assimilation (DA) is quite important, especially for regions for which airborne Doppler radar observations are not available.

In recent years, the impact of assimilating coastal Doppler radar observations on landfalling TC track and intensity forecasts has been widely examined using ensemble Kalman filter (EnKF) DA (Zhang et al., 2009; Weng et al., 2011; Dong and Xue, 2013; Wang et al., 2014; Zhu et al., 2016). For example, Zhang et al. (2009) assimilated coastal Doppler radar observations into a WRF-based EnKF, and their results demonstrated that the EnKF system greatly improved the initialization and forecast of the rapid formation and intensification of Hurricane Humberto (2007).

Although the EnKF assimilation of coastal radar observations has been proven to be a promising approach in improving the forecasting of TC track and intensity, research with respect to its impact on TC rainfall forecasting is very limited. Recently, Wang et al. (2014) investigated the impact of assimilating Taiwan coastal radar data for a landfalling typhoon [Jangmi (2008)] using an ARPS-based EnKF system. Encouragingly, their results showed that the forecasts for TC track, intensity, structure, and rainfall were improved, after

* Corresponding author: Zhiyong MENG
Email: zymeng@pku.edu.cn

assimilating the horizontal winds retrieved via the "TC circulation tracking radar echo correlation technique". However, very few studies have examined the impact of assimilating original Vr data on landfalling TC rainfall forecasts using an EnKF. Wang et al. (2014) tried to assimilate Vr data but did not obtain any apparent improvement. Zhu et al. (2016) examined the impact of assimilating Vr data from Guangzhou radar on the forecast of Typhoon Vicente (2012), which is the only paper in the literature (to the best of the authors' knowledge) that used coastal radar EnKF DA and improved the rainfall forecast of a landfalling typhoon.

Another limitation on coastal radar EnKF DA is that there is a severe lack of studies in the literature on the impact of coastal radar observability on landfalling TC simulation. Data coverage changes with the approach of the landfalling TC. How long before the TC makes landfall and how many radars should be assimilated to give a better forecast remain unanswered questions. Another open question relates to the verification of the radar DA results. Most studies use unassimilated Vr observations of a single radar for verification (e.g., Zhang et al., 2009; Dong and Xue, 2013). However, whether this is a reasonable approach has not yet been examined. This study set out to answer these three questions using a WRF-based EnKF for Typhoon Morakot (2009).

During 6–9 August 2009, Typhoon Morakot brought the most rainfall recorded in 50 years (approaching 3000 mm in 4 days) to the mountainous region of southern Taiwan. It made landfall near Hua-Lien on the east coast of Taiwan at around 1800 UTC 7 August 2009, and thereafter moved very slowly towards the north-northwest. Intense rainfall occurred in southern Taiwan, with the maximum 24-h rainfall amount reaching 1345.5 mm, which is not far from the world record of 1825 mm (Zhang et al., 2010). The heavy rainfall triggered massive mudslides and severe flooding (Wu and Yang, 2011; Wu, 2013), which made Morakot the deadliest typhoon to impact Taiwan in recorded history. It caused fatalities of more than 700 and direct economic losses exceeding $3.8 billion (Wang et al., 2012).

Since the occurrence of Typhoon Morakot (2009), relative to many efforts made regarding the contributing factors to extremely heavy rainfall through observational analyses or numerical simulations (Hong et al., 2010; Chien and Kuo, 2011; Fang et al., 2011; Huang et al., 2011; Liang et al., 2011; Van Nguyen and Chen, 2011; Wu et al., 2011; Wang et al., 2012; Yu and Cheng, 2013, 2014), studies on how the accuracy of rainfall forecasts can be improved have been very limited. Yen et al. (2011) examined the impact of storm translation speed on the rainfall simulation of Morakot by directly assimilating the tracks of a hurricane-like vortex using a WRF-based EnKF, and showed that a 55% increase of the storm translation speed led to a 33% reduction in the maximum accumulated rainfall in southern Taiwan. Schwartz et al. (2012) assimilated satellite-measured microwave radiances based on a cyclic, limited-area ensemble adjustment Kalman filter and found that, although a better intensity forecast could be obtained by radiance assimilation, the impact on typhoon track and rainfall forecasts was unsubstantial and mixed. To date, the impact of assimilating coastal radar data on the rainfall forecast of Typhoon Morakot (2009) has not been examined.

The objective of this study was to explore the impact of assimilating Vr observations from coastal Doppler radars on the track and rainfall forecasts in the Taiwan area, as Typhoon Morakot (2009) made landfall, using a WRF-based EnKF system. In particular, we set out to answer to what extent the track and rainfall forecasts of Typhoon Morakot (2009) could be improved by radar EnKF DA. This was approached using sensitivity experiments and detailed analyses, based on various DA strategies with respect to the radar observability and the start time and length of DA. We chose to assimilate Vr rather than reflectivity because radar reflectivity has much lower correlation with model variables than Vr, and thus assimilating radar reflectivity may not contribute much more to the performance of the EnKF (Dowell et al., 2011; Dong and Xue, 2013).

In section 2, the model configuration, the EnKF technique, the processing of the observations to be assimilated, and the design of the DA experiments are introduced. Section 3 presents the performance of the control experiment by assimilating Vr data from all the four Taiwan coastal Doppler radars during the 6 h immediately before TC landfall, in terms of typhoon track and rainfall forecasts. The sensitivity of the EnKF's performance to the radar observability and the start time and length of DA is presented in sections 4 and 5. A summary and conclusions are given in section 6.

2. Data and methodology

2.1. *WRF and EnKF*

The model used in this study was the Advanced Research version of WRF, version 3.6.1 (Skamarock et al., 2008). Three domains (D1, D2 and D3) with two-way nesting were used, with 150×110, 172×151 and 250×250 grid points in the longitudinal and latitudinal direction, respectively, and grid spacings of 40.5, 13.5 and 4.5 km (Fig. 1a). All domains had 35 vertical layers, and the model top was set at 10 hPa. The physical parameterization schemes included the improved Grell-3D ensemble cumulus scheme (Grell and Dévényi, 2002) for the two coarse domains (D1 and D2), the WRF Single-Moment six-class microphysics with graupel (Hong et al., 2004), and the Yonsei State University scheme (Noh et al., 2003) for planetary boundary layer processes. The initial and boundary conditions were provided by the $0.5^\circ \times 0.5^\circ$ NCEP GFS operational analysis and its three-hourly forecast.

The WRF-EnKF system used in this study was the same as that in Zhang et al. (2009) and Weng and Zhang (2012), which was originally developed for regional scale DA in Meng and Zhang (2008a, b). The ensemble size was 60. As in Zhang et al. (2006), the initial ensemble was generated with the WRF three-dimensional variational DA (3DVar) using the default cv3 background error covariance option (Barker et al., 2004). The initial uncertainties, represented by the domain-

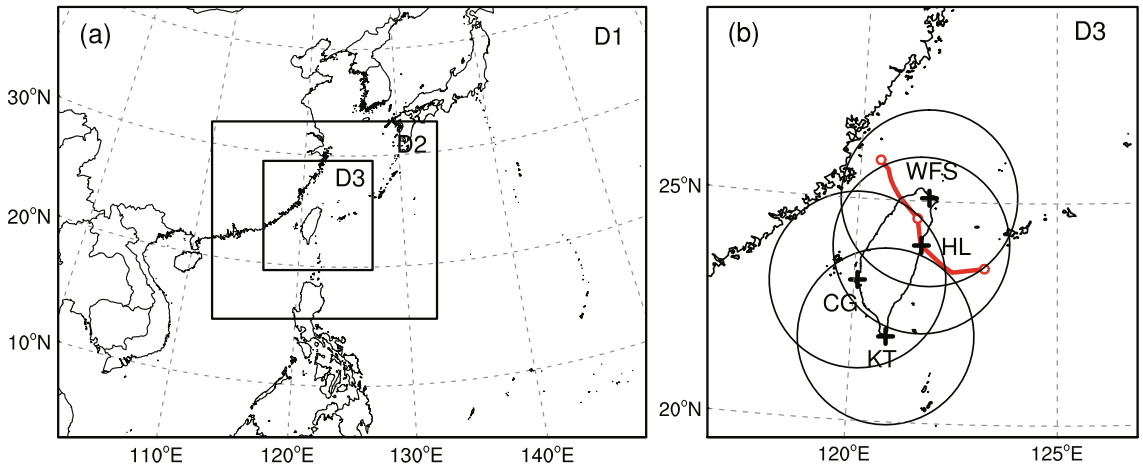

Fig. 1. (a) Model domain configuration. (b) An enlargement of the innermost domain (D3). The red line denotes the CWB best track of Typhoon Morakot (2009) from 0000 UTC 7 August to 0000 UTC 9 August 2009. All the positions at 0000 UTC are marked by a white dot. Also shown are the locations (black "+") and names of the four operational radars in Taiwan, along with their respective maximum Doppler ranges (black circles).

averaged standard deviation of the perturbed variables, were 2.14 m s^{-1} and 2.11 m s^{-1} for the horizontal wind components (u,v), 1.02 K for potential temperature, 101.45 Pa for pressure perturbation, and 0.51 g kg^{-1} for the water vapor mixing ratio. DA was performed for all domains. The covariance relaxation method (Zhang et al., 2004) was used to prevent filter divergence. This method inflates the covariance via a weighted average between the prior perturbation (denoted by the subscript f) and the posterior perturbation (denoted by the subscript a) as $(x_{a,new})' = (1-\alpha)(x_a)' + \alpha(x_f)'$, and the coefficient α was set to 0.8, which was the same as that in Zhang et al. (2009). The successive covariance localization method proposed by Zhang et al. (2009) was also used to respectively reduce the multiscale errors of the atmosphere. As in Zhang et al. (2009), 10% of the total radar observations were first randomly sampled and assimilated with a horizontal localization radius of influence (ROI) of 1215 km in all three domains. Then, another 20% of the observations were assimilated with an ROI of 405 km in D2 and D3. Finally, another 60% of the observations were assimilated using an ROI of 135 km, in D3 only. The remaining 10% of the observations that were not assimilated were used for verifications.

2.2. *Radar data processing and superobservations*

In this study, Vr data from four S-band (10 cm) coastal Doppler radars, which are operated by the Central Weather Bureau (CWB) of Taiwan, were used. These radars are located at the sites of Wu-Fen-Shan (WFS), Ken-Ting (KT), Hua-Lien (HL), and Chi-Gu (CG) (Fig. 1b). All of them are operated in the same volume coverage pattern "21" scanning mode of WSR-88D, consisting of nine elevation angles between 0.5° and 19.5° and having a 230 km maximum Doppler range. The data quality control was first conducted manually on each radar, including the removal of erroneous observations and velocity dealiasing using the NCAR SOLO software (Nettleton et al., 1993). Given the much higher resolution of radar observations than the model grid spacing, superobservations (SOs) were generated using the procedure developed by Zhang et al. (2009), for assimilation by the EnKF. The evolution of both the total number of assimilated SOs and the distribution of Vr data from different radars are shown in Fig. 2. The observational error of the SOs was assumed to be 3 m s^{-1}, which is the same as that used in previous studies (e.g., Zhang et al., 2009; Weng and Zhang, 2012).

2.3. *Experimental design*

Three groups of DA experiments were performed, as shown in Fig. 3, to examine the impact of assimilating Vr data from multiple versus a single radar at different locations relative to Typhoon Morakot with different DA start times and lengths. The benchmark forecast without assimilating observations (NoDA) was initiated from the NCEP GFS analysis at 0000 UTC 7 August 2009 (Fig. 3a).

In the first group (Fig. 3b), the initial ensemble was first integrated for 12 h, from 0000 to 1200 UTC 7 August, to develop an approximately realistic, flow-dependent background error covariance structure. SOs from all four radars and each single radar were then assimilated hourly from 1200 to 1800 UTC 7 August, spanning the 6 h immediately before Typhoon Morakot made landfall in Taiwan. The following 24-h deterministic forecasts were initiated from the ensemble mean of the EnKF analyses. Since the time between assimilating the first observation and Morakot's landfall was 6 h, this group was suffixed by "L6DA6", and named as All_L6DA6, WFS_L6DA6, HL_L6DA6, CG_L6DA6, and KT_L6DA6, respectively, for assimilating all the four radars and the single radars of WFS, HL, CG and KT. All_L6DA6 was used as the control experiment.

The second group was designed to examine the impact of an earlier DA start time with the same DA length (Fig. 3c). It was configured the same as the first group, except that the initial ensemble was integrated for only 6 h; thus, the DA was

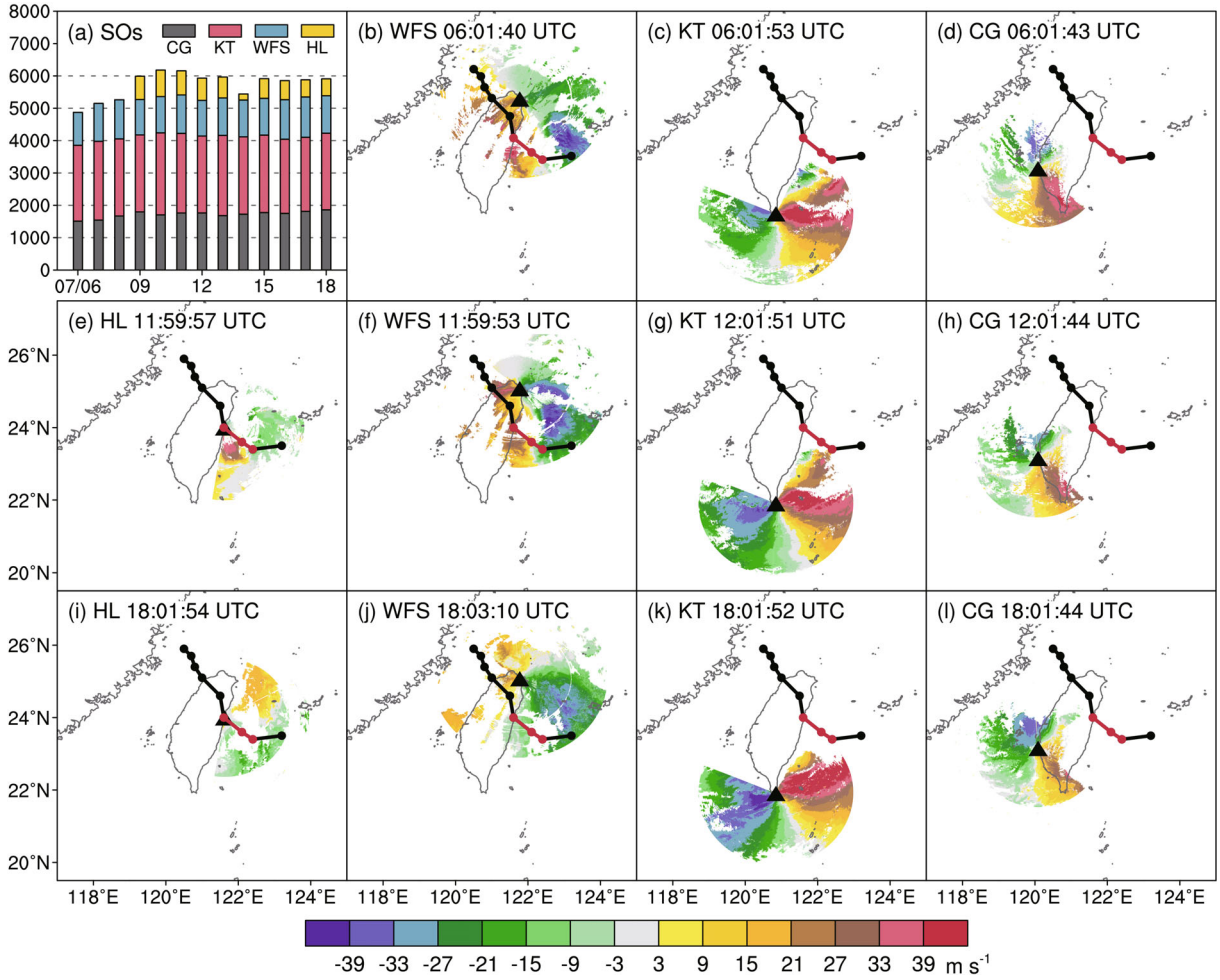

Fig. 2. (a) The number of SOs from each radar during the assimilation period. Also shown are the distributions of Doppler Vr (units: m s^{-1}) at the 0.5° elevation angle for (e, i) HL, (b, f, j) WFS, (c, g, k) KT, and (d, h, l) CG at around (from upper to lower) 0600, 1200 and 1800 UTC 7 August 2009. The locations of each radar (black triangle) and the six-hourly CWB best track from 0000 UTC 7 August to 0000 UTC 9 August (the red segment denotes the assimilation period) are also plotted.

performed 12 h ahead of Morakot's landfall and lasted for 6 h. The deterministic forecasts were initiated from the ensemble analysis mean at 1200 UTC 7 August. This group was named with the suffix "L12DA6".

The third group was the same as the second group, except that the DA lasted for 12 h and the deterministic forecasts were initiated at 1800 UTC 7 August (Fig. 3d). This group was named with the suffix "L12DA12". There were only three single-radar DA experiments in the latter two groups due to a lack of observations at the HL radar from 0600 to 0800 UTC 7 August (Fig. 2a). Vr data from all available radars were assimilated in All_L12DA6 and All_L12DA12, including the HL radar data during 0900 to 1800 UTC 7 August, whose amount was much smaller than for the other three radars.

3. Impact of radar DA in the control experiment All_L6DA6

Assimilating all four radars during the 6 h immediately before TC landfall decreased the RMSE of Vr relative to NoDA by about 58% at the end of the final EnKF cycle (black dashed line in Fig. 4a). In this study, we used a formula to quantitatively evaluate the improvement contributed by radar DA, as follows:

$$I = \frac{X_{\mathrm{NoDA}} - X_{\mathrm{DA}}}{X_{\mathrm{NoDA}}},$$

where X_{DA} and X_{NoDA} denote the variables [e.g., the RMSE of Vr, the track error, and the threat score (TS) of rainfall] with and without DA, respectively. The Vr was verified against the independent SOs from all four radars, each of which provided the same number of randomly chosen unassimilated SOs.

The simulated TC track in the deterministic forecast initiated from the ensemble analysis mean at 1800 UTC 7 August was significantly improved compared to NoDA (Figs. 5b and d). Due to the influence of the mountainous terrain of Taiwan Island, the low-level circulation (e.g., 850 hPa) could not be used to locate the TC center. In this study, the position of the simulated TC was determined by averaging the TC circulation centers at the 700- and 500-hPa pressure

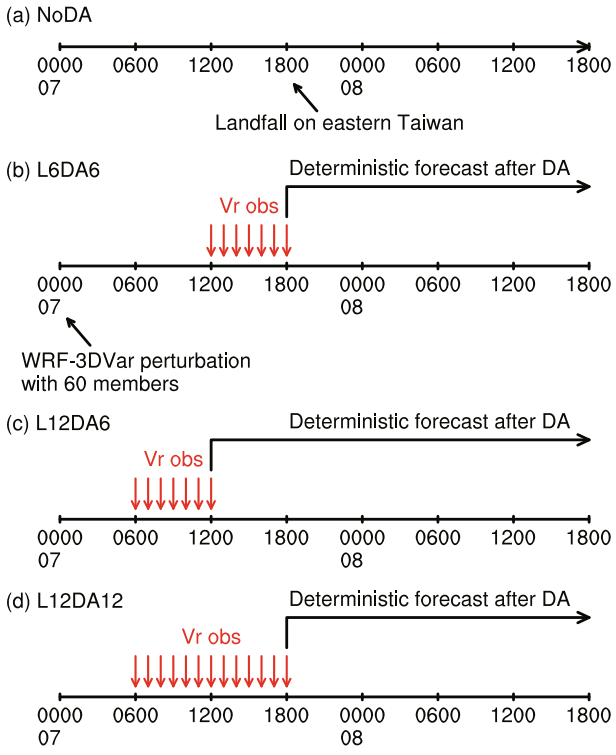

Fig. 3. Schematic flow chart for the (a) NoDA, (b) L6DA6, (c) L12DA6 and (d) L12DA12 groups.

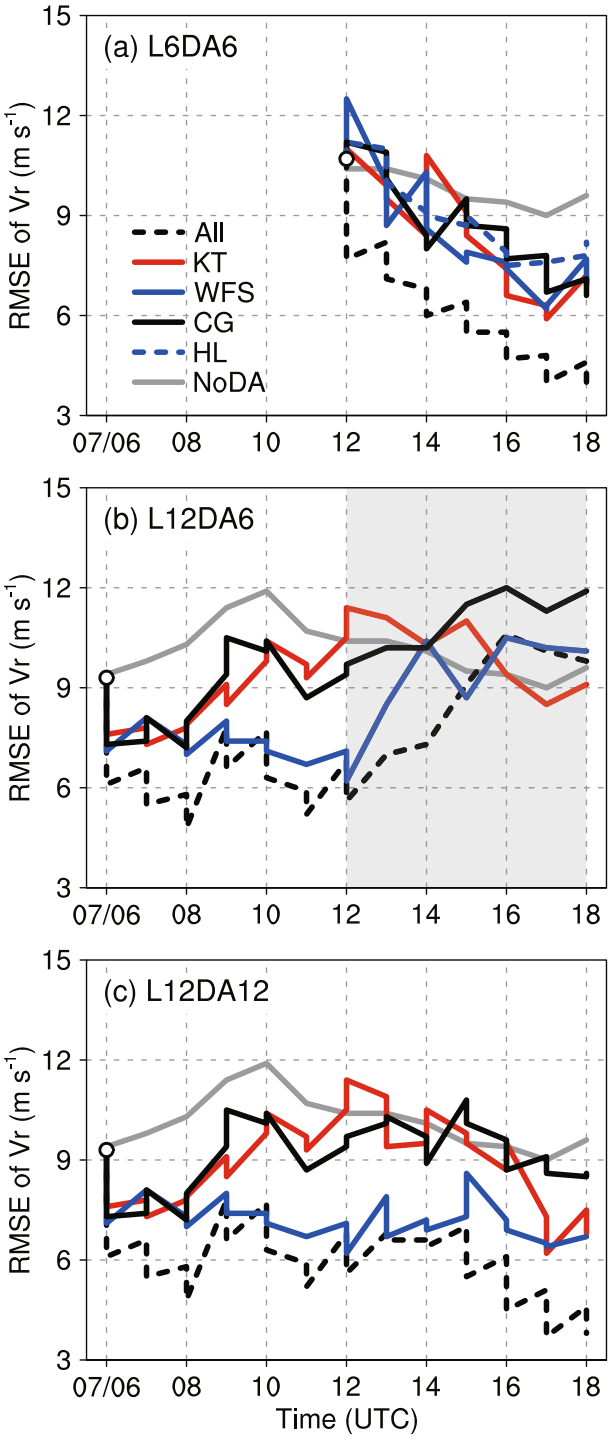

Fig. 4. The evolution of the prior and posterior RMSE of Vr (units: m s^{-1}) for the multiple- and single-radar DA experiments in the (a) L6DA6, (b) L12DA6 and (c) L12DA12 groups during 0600–1800 UTC 7 August 2009. The legend is shown in (a). The gray shading in (b) denotes the deterministic forecast period.

levels. In NoDA, the predicted typhoon had a late landfall time and moved northward slower than the observed track (Fig. 5b). With the assimilation of Vr data from all four radars, the simulated typhoon obtained a translation speed that was quite similar to the observed one (Fig. 5d). The mean track error during 1800 UTC 7 August to 1800 UTC 8 August (hereafter referred to as the track error, unless otherwise specified) decreased from 79.8 km in NoDA to 45.1 km in All_L6DA6 (improved by about 43%; Fig. 6a).

All_L6DA6 produced a more accurate forecast of the 24-h rainfall starting from 1800 UTC 7 August (hereafter referred to as 24-h rainfall, unless otherwise specified) than NoDA. The observed heavy rainfall exceeding 800 mm mostly concentrated in southwestern Taiwan, with several maximum centers located over the mountainous areas (Fig. 5a; interpolated using the rain gauge data). A southward bias of the heavy rainfall region was observed in NoDA (Fig. 5b). Assimilating all four radars during 1200–1800 UTC 7 August improved the 24-h rainfall forecast compared to NoDA in terms of both the rainfall pattern and the averaged TS. In All_L6DA6, the rainfall coverage extended more to the north in various thresholds from 100 to 1000 mm (Fig. 5d). The TS of the 24-h rainfall averaged over the 600-, 800- and 1000-mm thresholds increased from 0.18 in NoDA to 0.46 in All_L6DA6 (almost tripled; Fig. 6b).

The better rainfall forecast in All_L6DA6 was found to be closely associated with the stronger moisture flux more to the north compared to NoDA. Considering the south–north-oriented mountain barrier of southern Taiwan, which implies the importance of the westerly wind component in the context of the terrain–airflow interaction, and the important role of southwesterly flow in contributing to the orographic enhancement of precipitation in southern Taiwan, the evolution

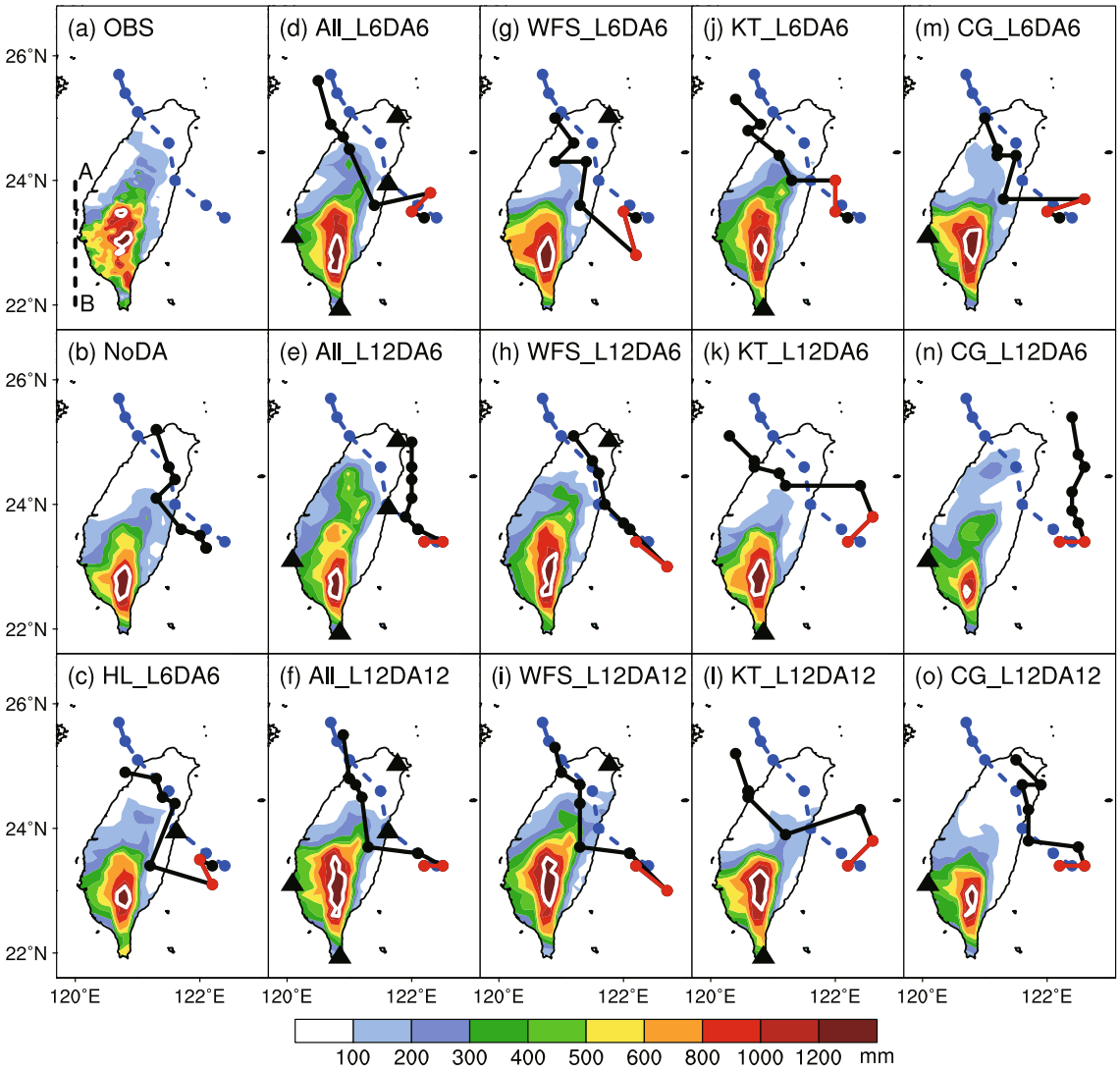

Fig. 5. (a) Observational analysis of the 24-h rainfall (units: mm) starting from 1800 UTC 7 August 2009 over Taiwan Island, (b) the corresponding forecast of NoDA, and the deterministic forecasts in the L6DA6, L12DA6 and L12DA12 groups, which assimilated Vr data from (c) HL, (d–f) all the available radars, (g–i) WFS, (j–l) KT, and (m–o) CG. The white contour in each panel denotes the 1200-mm heavy rainfall. The blue dashed and black solid lines with dots represent the observed and simulated track during 0600 UTC 7 August to 1800 UTC 8 August, respectively, with the red segment denoting the prior and posterior TC positions in the first EnKF cycle. The triangles denote the locations of the assimilated radars. The dashed line AB in (a) is the cross section used in Fig. 7.

of the upstream zonal moisture transport towards southern Taiwan was examined. The moisture flux was first integrated from the surface to 700 hPa to represent the integral moisture transport of the low-level atmosphere, and then the hourly moisture transport across 120°E (line AB in Fig. 5a) was calculated over the period of the 24-h rainfall. In NoDA, the strong low-level moisture transport exceeding 1000 kg m^{-1} s^{-1} was persistently located between 22°N and 23°N (Fig. 7a), which corresponded well with the latitude of heavy rainfall over Taiwan Island (Fig. 5b). To clearly demonstrate the impact of Vr DA on the moisture transport, the difference of zonal moisture flux between All_L6DA6 and NoDA is shown in Fig. 7b. A persistent larger moisture transport increment north of 23°N was observed in All_L6DA6, whereas the moisture transport south of 23°N did not change much, which was consistent with the northward expansion of the heavy rainfall region in All_L6DA6 (Fig. 5d).

The contribution to the rainfall forecast of assimilating radar data was also clearly reflected in the rainband structure. During and after Morakot's landfall, an east–west-oriented rainband was nearly stationary for around 15 h, before slowly moving northward at 1500 UTC 8 August (Figs. 8a–d). This quasi-stationary rainband extended from the Taiwan Strait to southwestern Taiwan and maintained at around 23°N, corresponding well with the latitude of heavy rainfall over Taiwan Island (Fig. 5a). Previous studies have partially attributed the torrential rainfall to this quasi-stationary rainband via observational analysis (e.g., Chien and Kuo, 2011; Yu and Cheng, 2013).

It was interesting to see how assimilating radar data may

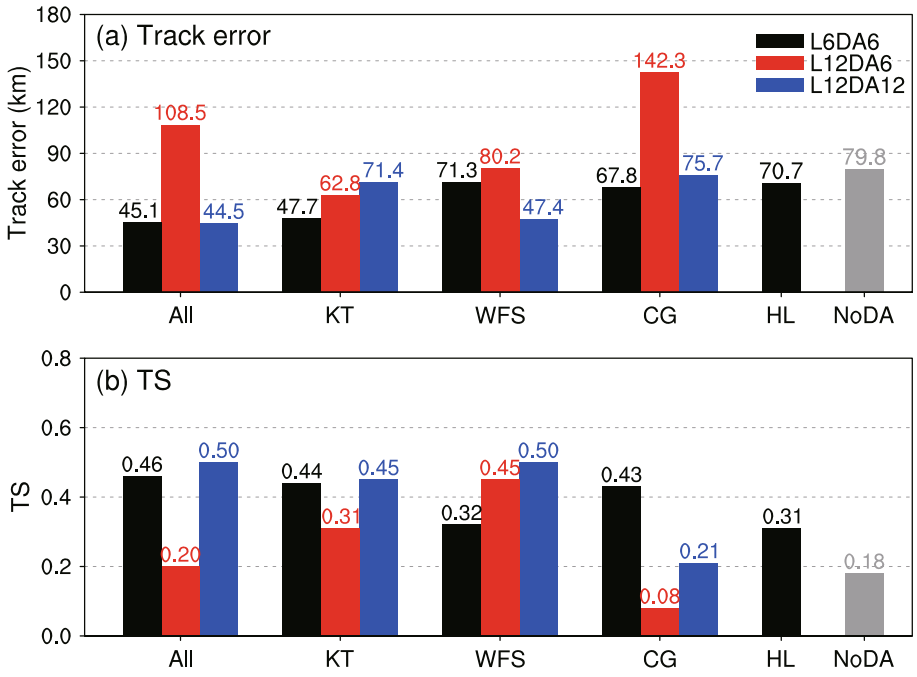

Fig. 6. (a) The 24-h mean track error and (b) the TS of 24-h rainfall averaged over the 600-, 800- and 1000-mm thresholds of the NoDA, multiple- and single-radar DA experiments in the L6DA6, L12DA6, and L12DA12 groups during 1800 UTC 7 August to 1800 UTC 8 August 2009. The legend is shown in (a).

help to improve the simulation of the abovementioned quasi-stationary rainband. The results showed that NoDA failed to reproduce it (Figs. 8m–p). However, assimilating Vr data from all four radars successfully reproduced the evolutionary features of the rainband in terms of both morphology and location, as well as the structural pattern of the entire typhoon circulation (Figs. 8e–h), although it somewhat overestimated the strength of the rainband. Behind the better simulation of the rainband was the better captured convergence line corresponding to the rainband to the southwest of Taiwan Island (Figs. 9a–d versus i–l). It has been suggested that the convergence line was a result of the interaction between Morakot's circulation and the southwesterly monsoonal flow active over the South China Sea (Yu and Cheng, 2014).

4. Sensitivity to the radar observability

To examine the impact of radar observability, four single-radar DA experiments were performed using exactly the same assimilation window as that of All_L6DA6. The results showed that the RMSEs of Vr in the four single-radar DA experiments at the end of the assimilation window all decreased compared to that in NoDA (Fig. 4a). They were, however, all larger than that in All_L6DA6. Consistent with the Vr analyses, all four experiments produced a track forecast error smaller than that of NoDA but larger than that of All_L6DA6 (Fig. 6a). The same was also true in terms of the TS of the 24-h rainfall forecast (Fig. 6b), likely because the moisture transport north of 23°N in the single-radar DA experiments was generally stronger than that in NoDA but weaker than that in All_L6DA6 (Figs. 7c–f). All the single-radar DA experiments favored in varying degrees the recurrence of the quasi-stationary rainband and the associated low-level convergence line (e.g., KT_L6DA6; Figs. 8i–l, 9e–h).

Different performances were evident among different single-radar DA experiments. The improvement of the TC track forecast contributed by assimilating the KT radar was apparently larger than that achieved by assimilating other radars (Fig. 6a). Assimilating a radar in a quadrant of the TC circulation tended to push the TC center position away from the assimilated radar (Figs. 5c, g, j and m), probably because a larger wind increment occurred around the stronger winds observed by a radar and the surrounding regions induced by cross correlations (Figs. 2e–h and 10b–e). For example, the wind analysis increment in WFS_L6DA6 consisted of strong northeasterly wind in a wide area around the observed TC center (Fig. 10b), leading to a large southeastward bias of the analyzed TC position (Fig. 5g) and an apparent increase in the initial analyzed error of Vr (Fig. 4a). When the bias of the analyzed TC center was opposite (similar) to the general moving direction of the TC, the track forecast error was larger (smaller). Besides, as the errors of Vr in all the single-radar DA experiments decreased similarly during the assimilation period (Fig. 4a), the smallest first-time analyzed TC position error in KT_L6DA6 might have favored its most realistic TC center in the final EnKF analysis among all the single-radar DA experiments (Figs. 5c, g, j and m), contributing to its largest reduction of the subsequent deterministic TC track forecast error compared to NoDA (Fig. 6a).

Consistent with the improvement in the TC track forecast, the rainfall simulation in KT_L6DA6 was the best among

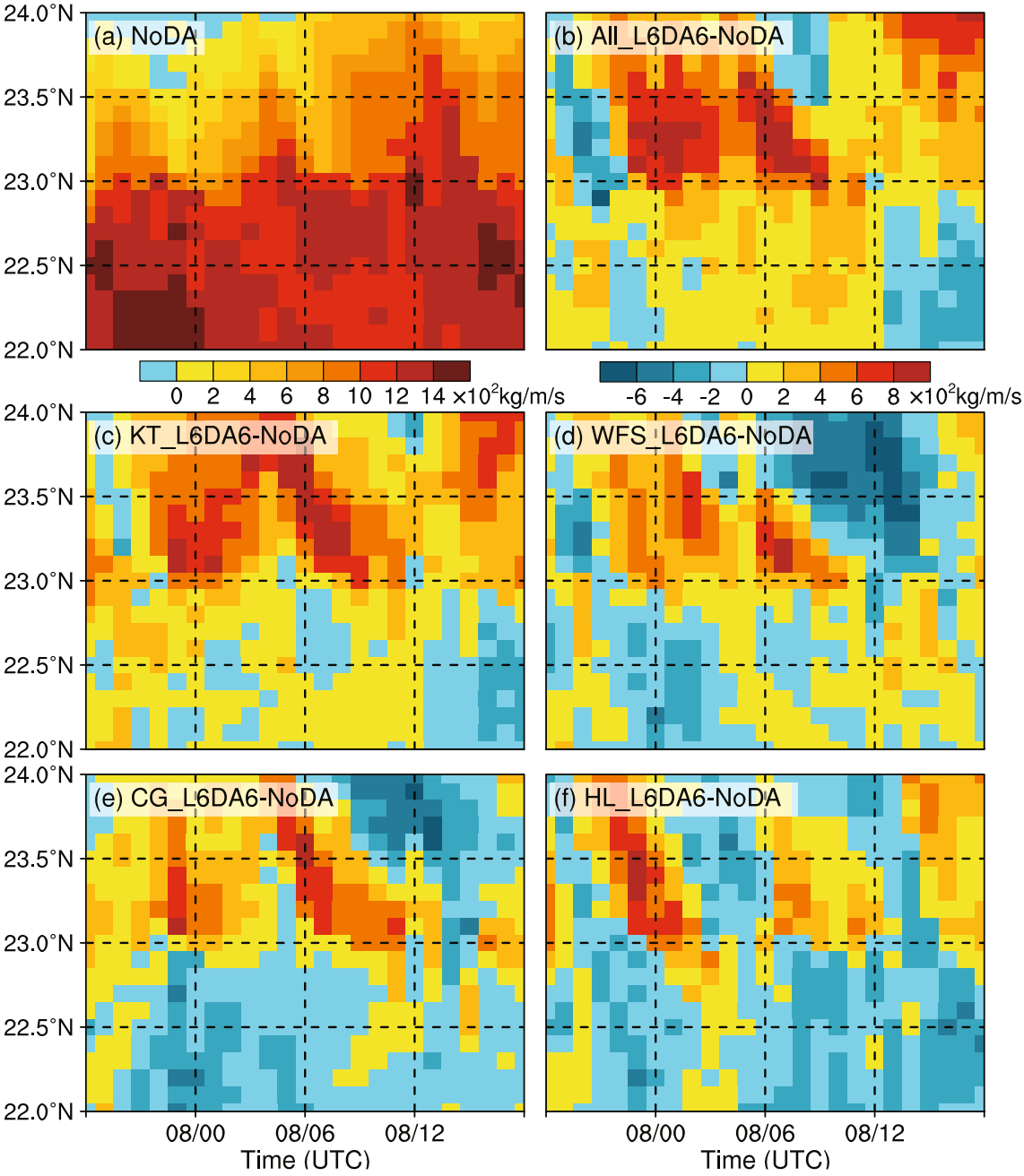

Fig. 7. Latitude–time plot of (a) the vertically integrated (from surface to 700 hPa) zonal moisture flux (units: kg m^{-1} s^{-1}) across 120°E (line AB in Fig. 5a) during 1800 UTC 7 August to 1800 UTC 8 August 2009 in NoDA, and that of the difference of vertically integrated zonal moisture flux (units: kg m^{-1} s^{-1}) across the same cross section between NoDA and (b) All_L6DA6, (c) KT_L6DA6, (d) WFS_L6DA6, (e) CG_L6DA6, and (f) HL_L6DA6.

all the single-radar DA experiments (Fig. 6). The persistent larger moisture transport increment north of 23°N in KT_L6DA6 favored its largest northward expansion of the heavy rainfall exceeding 200–800 mm (Figs. 5j and 7c). However, both the increment and decrement of moisture transport coexisted north of 23°N in the other three single-radar DA experiments, resulting in a relatively smaller northward expansion of the 200–800-mm heavy rainfall region (Figs. 5c, g and m, and 7d–f). Besides, it was found that the difference in the upstream zonal wind, rather than that of the moisture field, played a dominant role in the performance of the zonal moisture flux (figures not shown).

Aside from the above findings, it is important to note that the verification of Vr against multiple radars was more reasonable than against a single radar. It was found that assimilating Vr data from a single radar tended to decrease the error of Vr verified against the SOs provided by the same radar the most, but might have caused an increase of the error of Vr verified against other radars (Table 1). As a result, an experiment that produced the smallest error of Vr when verified against a single radar may not have produced the smallest error when verified against all the available radars, and also in

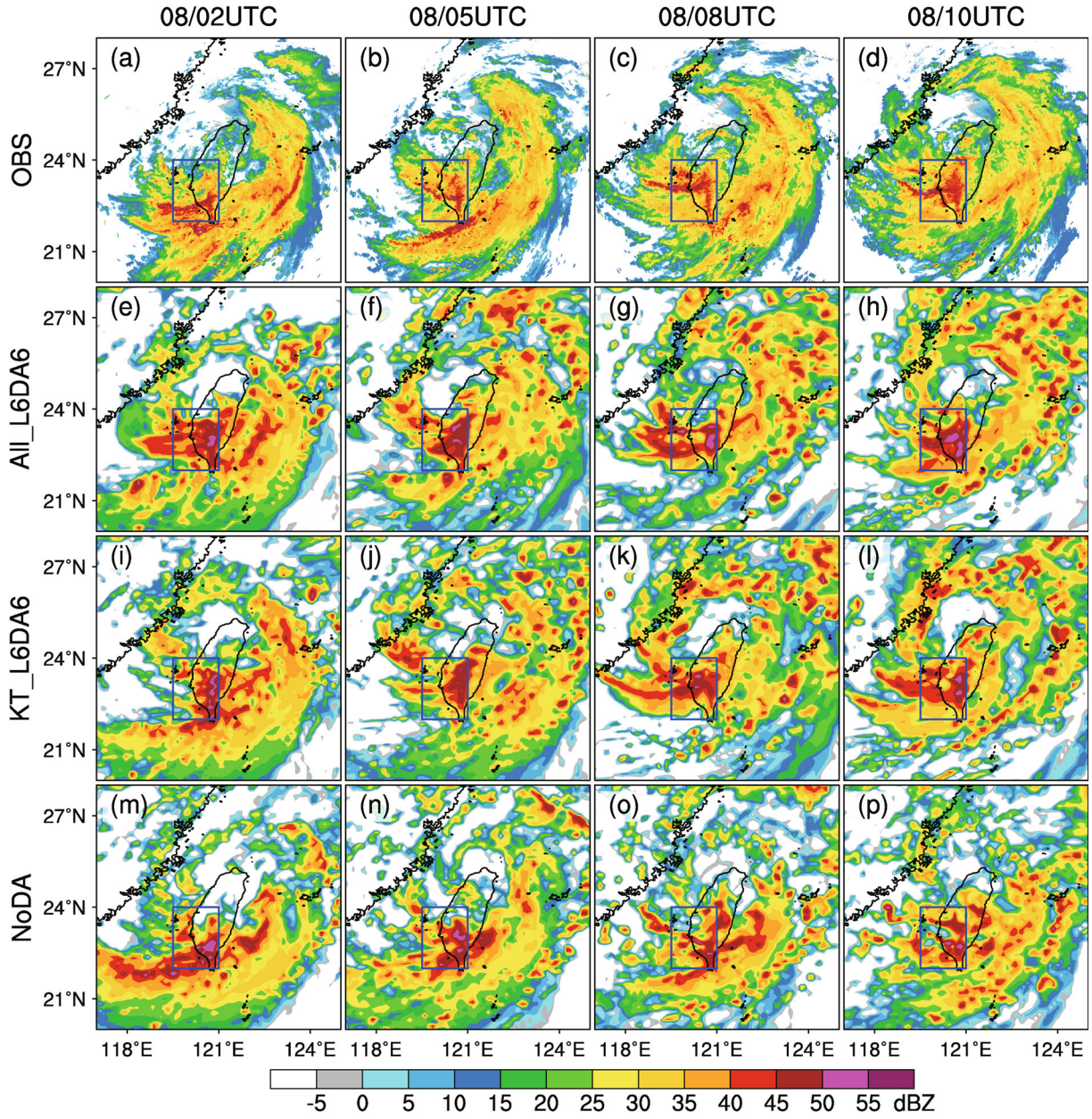

Fig. 8. The distribution of maximum radar reflectivity (units: dBZ) predicted by (e–h) All_L6DA6, (i–l) KT_L6DA6, and (m–p) NoDA, compared with (a–d) the observational composite mosaic at (from left to right) 0200, 0500, 0800 and 1000 UTC 8 August 2009. The inset box in each panel is used to locate the quasi-stationary rainband around the southwestern coast of Taiwan.

terms of the consequent TC track and rainfall forecasts. For example, when verified against the unassimilated SOs from the WFS radar, the analysis error of WFS_L6DA6 at 1800 UTC 7 August was 3.6 m s^{-1}, which was smaller than that of All_L6DA6 (4.0 m s^{-1}). However, when verified against the unassimilated SOs from all four radars, the analysis error of WFS_L6DA6 (6.9 m s^{-1}) was much larger than that of All_L6DA6 (4.0 m s^{-1}), which was consistent with the result that All_L6DA6 performed much better than WFS_L6DA6 in terms of both TC track and rainfall forecasts. Consequently, Vr should be verified using the observations from multiple radars, instead of a single radar, to avoid misinterpretation of the results.

Table 1. The posterior RMSE of Vr (units: m s^{-1}) at 1800 UTC 7 August 2009 in the L6DA6 group. The verification uses the unassimilated SOs from WFS, KT, CG, HL, and all four radars, respectively. The smallest value in each column is in bold and italic type.

	WFS	KT	CG	HL	All
WFS_L6DA6	***3.6***	8.9	6.9	7.3	6.9
KT_L6DA6	7.5	***3.4***	8.6	7.3	7.0
CG_L6DA6	6.3	8.1	***3.1***	7.6	6.6
HL_L6DA6	7.1	10.3	9.7	***4.1***	8.2
All_L6DA6	4.0	4.2	3.9	***4.1***	***4.0***
NoDA	7.8	9.4	10.4	10.7	9.6

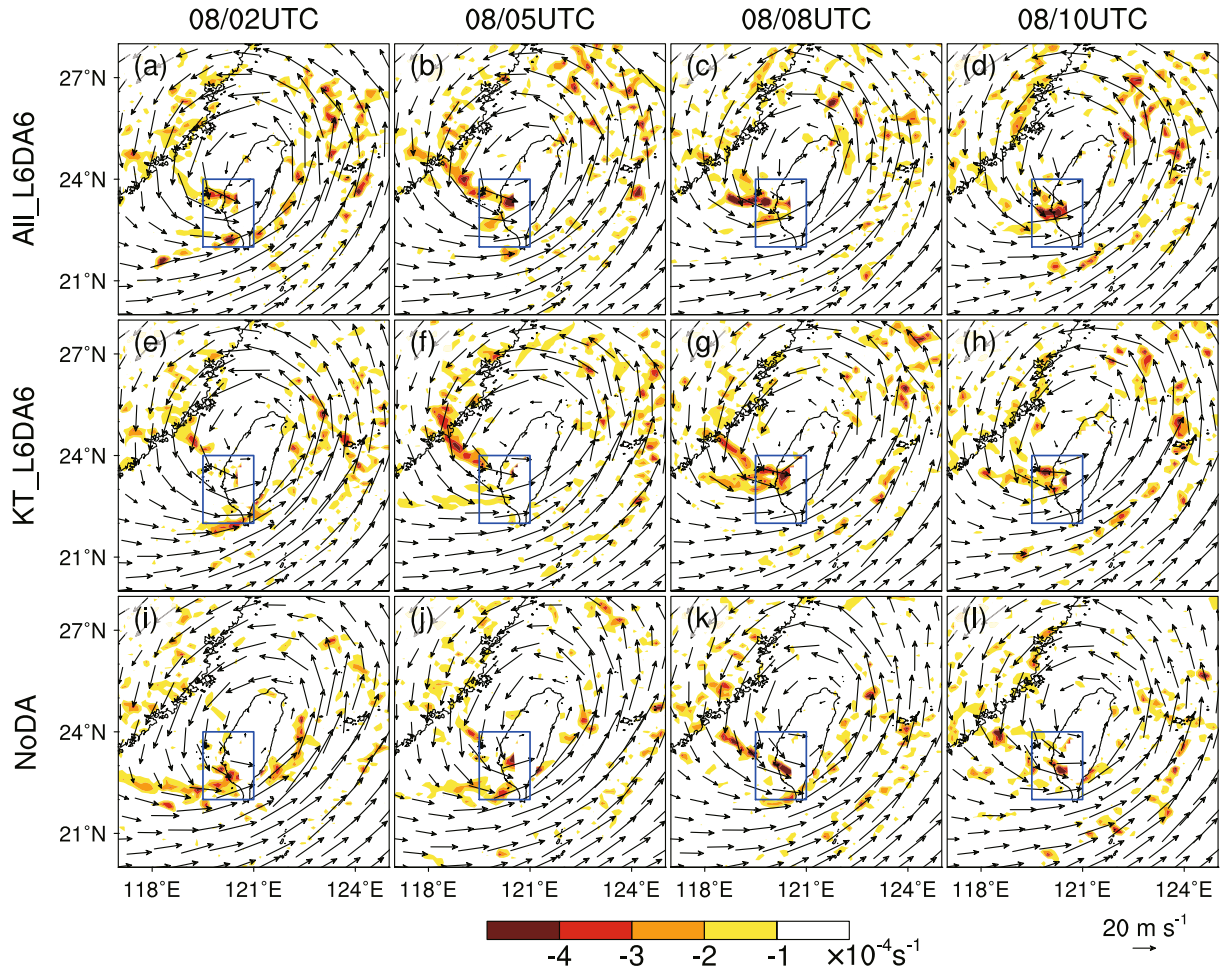

Fig. 9. The distribution of horizontal wind (units: m s^{-1}; reference vector in the lower-right corner) and wind divergence (units: s^{-1}; shaded) at 850 hPa predicted by (a–d) All_L6DA6, (e–h) KT_L6DA6, and (i–l) NoDA at (from left to right) 0200, 0500, 0800 and 1000 UTC 8 August 2009. The inset box in each panel is the same as that in Fig. 8.

5. Sensitivity to the start time and length of DA

In addition to how many radars and which radar may make the largest contribution to the track and rainfall simulation of Morakot, when and how long the DA should be performed are also important questions to answer. In this section, the performances of the experiments with different DA start times and lengths are presented and discussed.

5.1. *Assimilating all the available radars together*

Firstly, All_L12DA6 was implemented by shifting the 6-h assimilation window 6 h earlier to 0600–1200 UTC 7 August, to examine the impact of radar DA when the TC was farther away from making landfall (Fig. 3c). The results showed that, although the number of SOs did not change significantly (Fig. 2a), almost no improvement over NoDA was obtained by the DA at the time of landfall and in the following forecast (Figs. 5d and e). The error of Vr saturated after only 2 h into the EnKF cycling in All_L12DA6, followed by an apparent growth in the subsequent 6-h deterministic forecast, in contrast to the continuous error reduction of Vr in All_L6DA6 (black dashed line in Figs. 4a and b). The poor EnKF performance may be responsible for the result that the simulated TC in All_L12DA6 did not make landfall, and thus its track error was more than twice that in All_L6DA6 and was even larger than that in NoDA (Fig. 6a). The TS of the 24-h rainfall in All_L12DA6 decreased by more than half of that in All_L6DA6 and was similar to that in NoDA (Fig. 6b). These results indicate that assimilating coastal radar data during the 6 h immediately before TC landfall may have a much more positive and reliable impact on the track and rainfall forecasts after the TC made landfall than assimilating earlier observations.

The importance of assimilating Vr data within a few hours immediately before TC landfall was confirmed by the results in All_L12DA12, in which the assimilation window was extended to 1800 UTC relative to All_L12DA6 (Fig. 3d). In the extended 6-h assimilation window, the error of Vr decreased (Fig. 4c). At 1800 UTC, the error of Vr in All_L12DA12 was much smaller than that in All_L12DA6 and was almost the same as that in All_L6DA6. Similar improvement was also observed in terms of both TC track (Fig. 6a) and rainfall (Fig. 6b) forecasts.

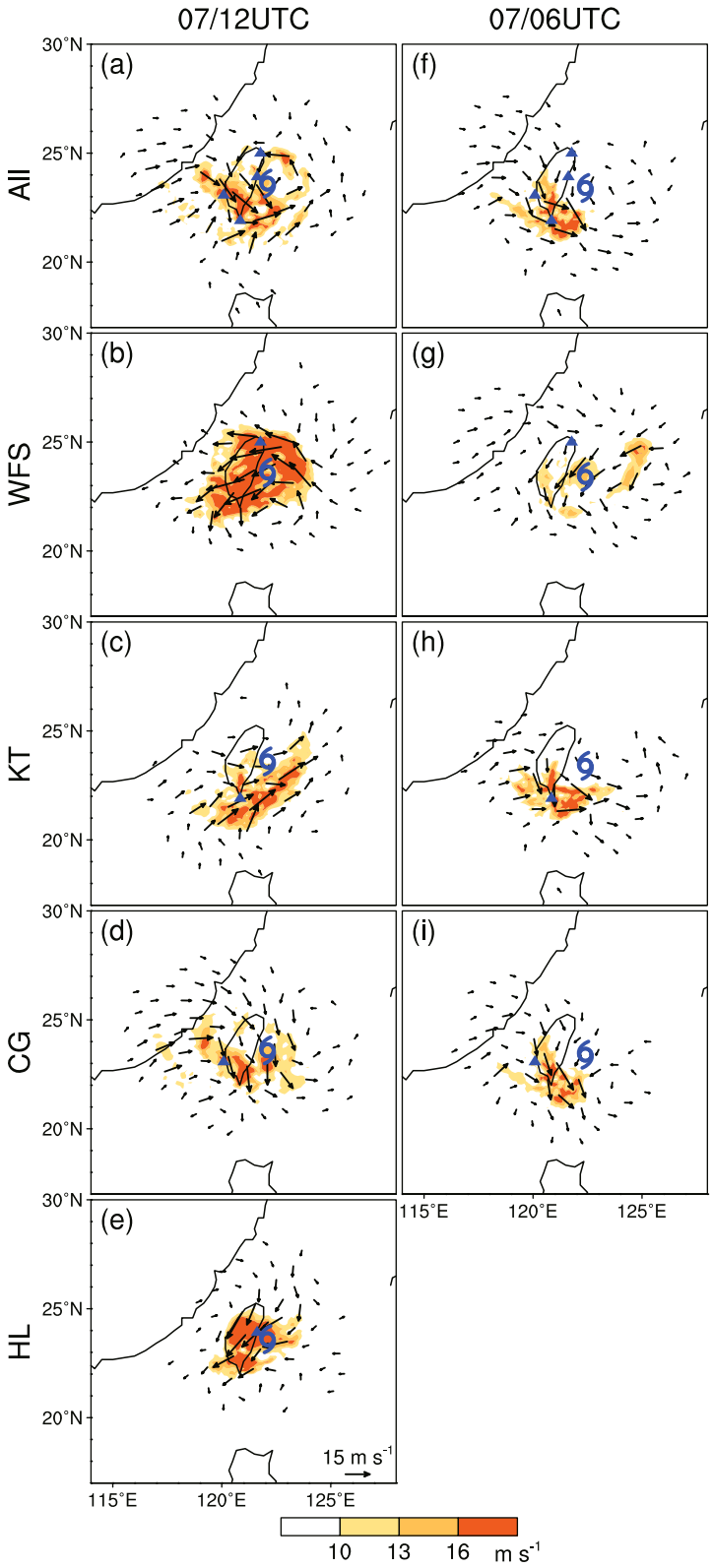

Fig. 10. The distribution of the wind analysis increment at 700 hPa (larger than 3 m s^{-1}) at (a–e) 1200 and (f–i) 0600 UTC 7 August 2009 by assimilating Vr data from (from top to bottom) all the available radars, WFS, KT, CG and HL. The shading denotes the magnitude of the wind increment (units: m s^{-1}) and the reference vector is in the lower-right corner of (e). The triangles and typhoon symbols represent the locations of the assimilated radars and the observed TC center, respectively.

5.2. *Assimilating a single radar individually*

Similar to the relative performance of multiple-radar DA experiments, the TC track forecast in the L12DA6 group was also worse than that in the L6DA6 group when only a single radar was assimilated (Fig. 6a). With different lengths of ensemble spin-up, the first-time wind analysis increment in these two groups had apparent differences. For example, the first-time wind analysis increment around the observed TC center in WFS_L12DA6 was much weaker than that in WFS_L6DA6 (Figs. 10b and g), likely because the shorter spin-up in WFS_L12DA6 led to the smaller background ensemble spread and thus smaller Kalman gain was given to the observation. Besides, KT_L12DA6 and CG_L12DA6 experienced error saturation and then error growth after 2-h of DA, while the wind error in WFS_L12DA6 was effectively reduced compared to NoDA by the EnKF cycles (Fig. 4b). In the first 6-h deterministic forecast, the errors of Vr either apparently increased or remained as large values, resulting in larger errors at 1800 UTC in the L12DA6 group than that in the L6DA6 group(Figs. 4a and b), which was consistent with the worse forecast performances in the former (Fig. 6). WFS_L12DA6 produced a similar TC track to the observation and thus a better rainfall forecast than WFS_L6DA6, although with a slower translation speed that led to a larger 24-h mean track error (Figs. 5g and h, and Fig. 6).

Extending the assimilation window by 6 h relative to the L12DA6 group improved TC track and rainfall forecasts (Fig. 6), except that the 24-h mean track error in KT_L12DA12 slightly increased due to the very unrealistic translation speed (Fig. 5l). The error growths of Vr during 1200–1800 UTC in the L12DA6 group were prevented in the L12DA12 group (Figs. 4b and c). At 1800 UTC, all the experiments in the L12DA12 group had smaller Vr errors than that in the L12DA6 group, probably due to the extended EnKF cycles. However, the improvement in terms of TC track and rainfall forecasts in CG_L12DA12 was very limited compared to NoDA, probably due to its comparable wind errors to NoDA during the assimilation period (Figs. 4c and 6).

Besides, the relative performance of single-radar DA experiments varied with the start time and length of DA. For example, assimilating WFS radar data contributed most to the improvement of the TC track and rainfall forecasts in the L12DA12 group, while assimilating KT radar data produced the best track and rainfall forecasts in the L6DA6 group. Consequently, assimilating all the available radars should be adopted so that the large uncertainty of benefits from a single radar can be eliminated.

6. Summary and conclusions

Through a WRF-based EnKF DA system, this study examined the impact of assimilating Vr observations from coastal Doppler radars on the track and 24-h torrential rainfall forecasts after Typhoon Morakot (2009) made landfall in Taiwan. The results showed that assimilating coastal radar data with a certain configuration significantly improved the track and rainfall forecasts of Morakot after landfall. The performance of radar EnKF DA may be apparently different for a change in the radar observability and the start time and length of DA.

It was found that assimilating Vr data from all four radars during the 6 h immediately before TC landfall was quite important for the track and rainfall forecasts after the TC made landfall. The TC track forecast error could be decreased by about 43% and the TS of the 24-h rainfall forecast could be almost tripled. The better rainfall forecast was closely related to the improved location of moisture transport, the quasi-stationary rainband, and the local convergence line. Assimilating multiple radars outperformed any single-radar DA experiment, likely because the local adjustment by assimilating a single radar tended to produce an unavoidable TC position error. Different radars might contribute to different degrees depending on the landfalling TC's track.

The improvement of DA apparently decreased when only Vr data obtained more than 6 h earlier than TC landfall were assimilated. However, assimilating Vr data continuously until TC landfall can regain the skillful track and rainfall forecasts. Besides, the relative performance of single-radar DA experiments varied with the start time and length of DA. Consequently, Vr data from all the available radars should be assimilated to achieve a better forecast performance.

Another important result was the choice of Vr data for verification. This work demonstrated that, instead of just a single radar, Vr data from all available radars should be used for a more reliable assessment of the EnKF performance. Verification against a single radar could easily be different from that against multiple radars, and may become inconsistent with the forecast performance, thus possibly causing misinterpretation of the results.

Considering that the above findings and conclusions were based on a single case only, it is necessary to be careful in generalizing the results. Nevertheless, the promising results in the current study may provide a useful reference on how to assimilate coastal radar data for improving the track and rainfall forecasts of a TC after landfall.

Acknowledgements. This work was sponsored by the Special Fund for Meteorological Research in the Public Interest from the Ministry of Science and Technology of China (Grant No. GYHY201306004), the National Key Basic Research Program of China (Grant No. 2013CB430104), and the National Natural Science Foundation of China (Grant Nos. 41461164006, 41375048 and 41425018). C.-K. YU and L.-W. CHENG were supported by the Ministry of Science and Technology of Taiwan (Grant No. MOST103-2111-M-002-011-MY3).

REFERENCES

Barker, D. M., W. Huang, Y. R. Guo, A. J. Bourgeois, and Q. N. Xiao, 2004: A three-dimensional variational data assimilation system for MM5: Implementation and initial results. *Mon. Wea. Rev.*, **132**, 897–914.

Chien, F.-C., and H.-C. Kuo, 2011: On the extreme rainfall of Ty-

phoon Morakot (2009). *J. Geophys. Res.*, **116**, D05104.

Dong, J. L., and M. Xue, 2013: Assimilation of radial velocity and reflectivity data from coastal WSR-88D radars using an ensemble Kalman filter for the analysis and forecast of landfalling hurricane *Ike* (2008). *Quart. J. Roy. Meteor. Soc.*, **139**, 467–487.

Dowell, D. C., L. J. Wicker, and C. Snyder, 2011: Ensemble Kalman filter assimilation of radar observations of the 8 May 2003 Oklahoma City supercell: Influences of reflectivity observations on storm-scale analyses. *Mon. Wea. Rev.*, **139**, 272–294.

Fang, X. Q., Y.-H. Kuo, and A. Y. Wang, 2011: The impacts of Taiwan topography on the predictability of Typhoon Morakot's record-breaking rainfall: A high-resolution ensemble simulation. *Wea. Forecasting*, **26**, 613–633.

Gao, S. Z., Z. Y. Meng, F. Q. Zhang, and L. F. Bosart, 2009: Observational analysis of heavy rainfall mechanisms associated with severe tropical storm Bilis (2006) after its landfall. *Mon. Wea. Rev.*, **137**, 1881–1897.

Grell, G. A., and D. Dévényi, 2002: A generalized approach to parameterizing convection combining ensemble and data assimilation techniques. *Geophys. Res. Lett.*, **29**, 38-1–38-4.

Hong, C.-C., M.-Y. Lee, H.-H. Hsu, and J.-L. Kuo, 2010: Role of submonthly disturbance and 40-50 day ISO on the extreme rainfall event associated with Typhoon Morakot (2009) in southern Taiwan. *Geophys. Res. Lett.*, **37**, L08805.

Hong, S. Y., J. Dudhia, and S.-H. Chen, 2004: A revised approach to ice microphysical processes for the bulk parameterization of clouds and precipitation. *Mon. Wea. Rev.*, **132**, 103–120.

Huang, C.-Y., C.-S. Wong, and T.-C. Yeh, 2011: Extreme rainfall mechanisms exhibited by Typhoon Morakot (2009). *Terrestrial*, *Atmospheric and Oceanic Sciences*, **22**, 613–632.

Liang, J., L. G. Wu, X. Y. Ge, and C.-C. Wu, 2011: Monsoonal influence on Typhoon Morakot (2009). Part II: numerical study. *J. Atmos. Sci.*, **68**, 2222–2235.

Meng, Z. Y., and F. Q. Zhang, 2008a: Tests of an ensemble Kalman filter for mesoscale and regional-scale data assimilation. Part III: comparison with 3DVar in a real-data case study. *Mon. Wea. Rev.*, **136**, 522–540.

Meng, Z. Y., and F. Q. Zhang, 2008b: Tests of an ensemble Kalman filter for mesoscale and regional-scale data assimilation. Part IV: comparison with 3DVar in a month-long experiment. *Mon. Wea. Rev.*, **136**, 3671–3682.

Nettleton, L., S. Daud, R. Neitzel, C. Burghart, W.-C. Lee, and P. Hildebrand, 1993: SOLO: a program to peruse and edit radar data. *Preprints*, *26th Conf. on Radar Meteorology*, Norman, OK, Amer. Meteor. Soc., 338–339.

Noh, Y., W.-G. Cheon, S.-Y. Hong, and S. Raasch, 2003: Improvement of the K-profile model for the planetary boundary layer based on large eddy simulation data. *Bound.-Layer Meteor.*, **107**, 401–427.

Schwartz, C. S., Z. Q. Liu, Y. S. Chen, and X.-Y. Huang, 2012: Impact of assimilating microwave radiances with a limited-area ensemble data assimilation system on forecasts of Typhoon Morakot. *Wea. Forecasting*, **27**, 424–437.

Skamarock, W. C., and Coauthors, 2008: A description of the advanced research WRF version 3. NCAR Tech. Note TN-475+STR, 113 pp.

Van Nguyen, H., and Y.-L. Chen, 2011: High-resolution initialization and simulations of Typhoon Morakot (2009). *Mon. Wea. Rev.*, **139**, 1463–1491.

Wang, C.-C., H.-C. Kuo, Y.-H. Chen, H.-L. Huang, C.-H. Chung, and K. Tsuboki, 2012: Effects of asymmetric latent heating on typhoon movement crossing Taiwan: the case of Morakot (2009) with extreme rainfall. *J. Atmos. Sci.*, **69**, 3172–3196.

Wang, M. J., M. Xue, K. Zhao, and J. L. Dong, 2014: Assimilation of T-TREC-Retrieved winds from single-Doppler radar with an ensemble Kalman filter for the forecast of Typhoon Jangmi (2008). *Mon. Wea. Rev.*, **142**, 1892–1907.

Weng, Y. H., and F. Q. Zhang, 2012: Assimilating airborne Doppler radar observations with an ensemble Kalman filter for convection-permitting hurricane initialization and prediction: Katrina (2005). *Mon. Wea. Rev.*, **140**, 841–859.

Weng, Y. H., M. Zhang, and F. Q. Zhang, 2011: Advanced data assimilation for cloud-resolving hurricane initialization and prediction. *Computing in Science & Engineering*, **13**, 40–49.

Wu, C.-C., 2013: Typhoon Morakot: key findings from the journal *TAO* for improving prediction of extreme rains at landfall. *Bull. Amer. Meteor. Soc.*, **94**, 155–160.

Wu, C.-C., and M. J. Yang, 2011: Preface to the special issue on "Typhoon Morakot (2009): observation, Modeling, and Forecasting". *Terrestrial*, *Atmospheric and Oceanic Sciences*, **22**, doi: 10.3319/TAO.2011.10.01.01(TM).

Wu, L. G., J. Liang, and C.-C. Wu, 2011: Monsoonal influence on Typhoon Morakot (2009). Part I: observational analysis. *J. Atmos. Sci.*, **68**, 2208–2221.

Yen, T.-H., C.-C. Wu, and G.-Y. Lien, 2011: Rainfall simulations of Typhoon Morakot with controlled translation speed based on EnKF data assimilation. *Terrestrial*, *Atmospheric and Oceanic Sciences*, **22**, 647–660.

Yu, C.-K., and L.-W. Cheng, 2013: Distribution and mechanisms of orographic precipitation associated with Typhoon Morakot (2009). *J. Atmos. Sci.*, **70**, 2894–2915.

Yu, C.-K., and L.-W. Cheng, 2014: Dual-Doppler-derived profiles of the southwesterly flow associated with southwest and ordinary typhoons off the southwestern coast of Taiwan. *J. Atmos. Sci.*, **71**, 3202–3222.

Zhang, F., C. Snyder, and J. Z. Sun, 2004: Impacts of initial estimate and observation availability on convective-scale data assimilation with an ensemble Kalman filter. *Mon. Wea. Rev.*, **132**, 1238–1253.

Zhang, F. Q., Z. Y. Meng, and A. Aksoy, 2006: Tests of an ensemble Kalman filter for mesoscale and regional-scale data assimilation. Part I: perfect model experiments. *Mon. Wea. Rev.*, **134**, 722–736.

Zhang, F. Q., Y. H. Weng, J. A. Sippel, Z. Y. Meng, and C. H. Bishop, 2009: Cloud-resolving hurricane initialization and prediction through assimilation of Doppler radar observations with an ensemble Kalman filter. *Mon. Wea. Rev.*, **137**, 2015–2125.

Zhang, F. Q., Y. H. Weng, Y.-H. Kuo, J. S. Whitaker, and B. G. Xie, 2010: Predicting Typhoon Morakot's catastrophic rainfall with a convection-permitting mesoscale ensemble system. *Wea. Forecasting*, **25**, 1816–1825.

Zhu, L., Q. L. Wan, X. Y. Shen, Z. Y. Meng, F. Q. Zhang, Y. H. Weng, J. Sippel, Y. D. Gao, Y. J. Zhang, and J. Yue, 2016: Prediction and predictability of high-impact western Pacific landfalling tropical cyclone Vicente (2012) through convection-permitting ensemble assimilation of Doppler radar velocity. *Mon. Wea. Rev.*, **144**, 21–43.